



Low-profile pattern reconfigurable patch antenna with dual bands characteristic for 5G NR communication

Zhonggen Wang¹, Jianguo Ma¹ , Wenyan Nie² and Weidong Mu¹

¹School of Electrical and Information Engineering, Anhui University of Science and Technology, Huainan, China and ²School of Mechanical and Electrical Engineering, Huainan Normal University, Huainan, China

Research Paper

Cite this article: Wang Z, Ma J, Nie W, Mu W (2024) Low-profile pattern reconfigurable patch antenna with dual bands characteristic for 5G NR communication. *International Journal of Microwave and Wireless Technologies*, 1–12. <https://doi.org/10.1017/S1759078724000874>

Received: 29 January 2024
Revised: 25 June 2024
Accepted: 29 June 2024

Keywords:

diverse patterns; dual band characteristics; near-field resonant parasitic unit; PIN diode

Corresponding author: Jianguo Ma;
Email: mjg1763119280@163.com

Abstract

In this paper, a low-profile antenna with characteristic of reconfigurable of dual bands' pattern for 5G New Radio (NR) communication is proposed to mitigate the problems of signal fading and multipath propagation. The design incorporates a turnstile-shaped patch, a circular patch with etched rectangular slots and a discontinuous ring patch. The circular patch with etched rectangular slots and discontinuous ring patch are placed in the same plane to obtain dual band characteristic. The discontinuous ring patch works as a near-field resonant parasitic unit to improve the front-to-back ratio values at the resonance points and adjust the beam direction. Eight diodes are loaded to control the connection states of the rectangle slots on the circular patch. By combining an electric dipole formed by diode-controlled slot with a magnetic dipole formed by the turnstile-shaped patch, then a dual-band antenna with diverse patterns is designed. The measured results show that the designed antenna has dual-band characteristics and operates in the bands of 3.39–3.62 GHz and 4.77–5.01 GHz with peak gains of 3.6 dBi and 4.2 dBi, respectively. Furthermore, the measured radiation pattern results show that it is feasible to reconfigure the pattern in both bands simultaneously at 45° intervals.

Introduction

In order to meet the diversified communication needs of modern society, and build a more efficient communication network, the continuously growing number of connected devices has prompted researchers to explore methods for achieving higher transmission rates and greater network capacity [1]. The fifth-generation wireless communication system (5G) matches the current trend of communication networks, while mainly using 3.3–3.6 GHz and 4.8–5.0 GHz as its communication frequency bands. However, 5G has severe multiple reflections, scattering, and uncertain communication coverage, especially for indoor and multi-obstacle scenarios. Meanwhile, it is essential to improve the existing issues of communication systems such as signal fading and multipath propagation. It has been reported that the above problems can be effectively solved by utilizing diversity technique and multipath combining technique. Antenna diversity techniques involve methods such as polarization diversity [2], frequency diversity [3], and pattern diversity [4, 5]. Pattern diversity is one of these specific implementations, focusing on the use of antenna radiation direction information to enhance signal reception performance. The utilization of pattern reconfigurable antennas, which can redirect the main beam to a specific direction, offers a number of benefits, such as better spatial multiplexing, interference reduction and suppression, counteracting multipath fading, and improved coverage [6]. Researchers have proposed several methods to implement the feature of reconfigurable radiation pattern. These methods can be generally categorized into two types according to the implementation principle. The first way is to obtain various radiation patterns by altering the structure of the antenna radiating element. In reference [7], a pattern reconfigurable antenna with two radiation patterns is designed by connecting two symmetrically distributed helical monopoles via switches. A multifunctional pattern reconfigurable antenna for 5G and higher applications is presented in reference [8]. The main beam direction of the antenna is tuned to +35°, 0°, and –35° by using diodes in a quarter-wavelength T-shaped director slot.

The second method is to load diodes on the feed network to obtain different types of feeding modes to realize multiple radiation patterns. A convenient fixed-frequency beam steering method is proposed in reference [9]. The researchers vary the feeding modes by controlling the voltage across the varactor diodes loaded on the feeding network. In reference [10], by switching two kinds of PIN diodes in the feeding network, three orthogonal characteristic modes are obtained, and then a multiple-input–multiple-output antenna with reconfigurable modes is fabricated out to verify its performance. Besides, a broadband reconfigurable feeding network is proposed in reference [11] to excite four identical arc dipoles and the experimental results show that the designed antenna can operate in four different modes with a radiation efficiency up to 60%. However, all of the above literatures have focused on implementing pattern

reconfigurable in single frequency band. The dual-band resonant characteristics of multiband antennas contribute to frequency multiplexing and higher transmission rates, which are needed for the 5G communications market. Therefore it is essential to realize the pattern reconfigurable in dual frequency bands. In references [12–15], researchers have achieved pattern reconfigurable in multiple frequency bands by using complementary antenna technique and loading parasitic structure technique. It is worth mentioning that, in reference [16], an arc-shaped strip which serves as a near-field resonant parasitic (NFRP) element is printed around a coplanar-waveguide-fed semiloop antenna to produce a peak gain and front-to-back ratio (FBR) values equal to 5.76 dBi and 12.67 dB, respectively. In reference [17], Yu et al. adopted a stacked structure scheme to enable the antenna operate in dual bands. The top and bottom patches are etched with rectangular slots of different lengths to allow the antenna to resonate in its two frequency bands. The turnstile-shaped patch works like a magnetic dipole and an electric dipole is introduced by etching rectangle slot on the top patch. Then, the combination of a magnetic dipole and an electric dipole achieves unilateral radiation. Meanwhile, the installation of diodes in the rectangular slots of the top patch makes the radiation pattern reconfigurable in low frequency band. Based on previous research, Zhou et al. have made the radiation patterns reconfigurable in both high and low frequency bands by etching slots on both top and bottom circular patch in reference [18].

In this paper, an antenna with reconfigurable radiation patterns in two frequency bands is researched and designed. The design provides a structurally optimized design for the stacked dual-band pattern reconfigurable antenna, which significantly reduces the complexity of the three-dimensional structure of this type of antenna. The designed antenna introduces only one excitation port, which is directly connected to a turnstile-shaped patch located in the middle layer through the center feed. Compared to references [17] and [18], the upper substrate structure is eliminated and a discontinuous ring patch is introduced around the ground plane as an NFRP unit. A set of rectangular slots are etched along the inside of the circular ground patch to improve impedance matching at the resonance points. Another set of rectangular slots are etched along the outside of the circular ground patch to change the current distribution and introduce electric dipoles to the antenna. In addition, two electric dipoles are introduced when the antenna resonates in the low and high frequency bands. Due to the principle of electromagnetic complementarity, unilateral radiation can be obtained in both bands. Then, eight bias circuits are assembled in eight rectangular slots to switch the electrical state of the rectangular slots. Finally, the radiation pattern of the slotted antenna can be reconstructed simultaneously in both high and low bands. The measurement results show that the impedance bandwidth of the antenna is 7.5% in the low frequency band and 5.1% in the high frequency band. Moreover, by switching the state of the PIN diode, eight radiation patterns are obtained in both bands, where the main beam radiates in the 0° , 45° , 90° , 135° , 180° , 225° , 270° , and 315° directions, respectively.

Antenna design and parametric analysis

Antenna geometry

The structure of the proposed pattern reconfigurable antenna is depicted in Fig. 1, and the dimensional parameters of the optimized antenna are shown in Table 1. As shown in Figs. 1(a) and (b),

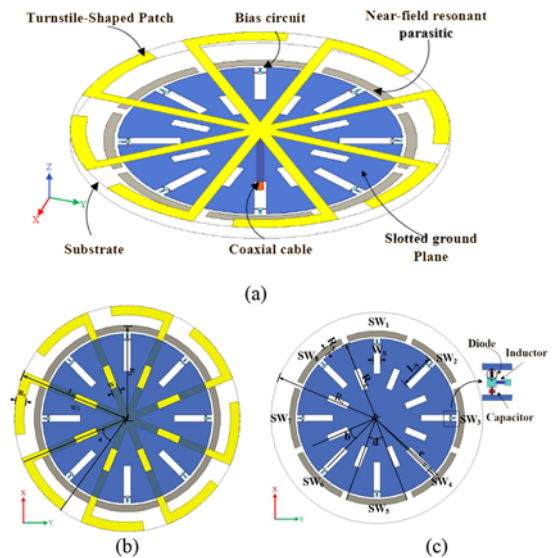


Figure 1. Configuration of the proposed pattern reconfigurable antenna. (a) 3-D view; (b) top view of the substrate; (c) bottom view of the substrate.

the proposed antenna consists of five main elements: a turnstile-shaped patch, a slotted ground structure, an NFRP unit, a substrate made of FR4-epoxy material ($\tan\delta = 0.02$) with a thickness of 1.6 mm and an SMA connector. A circular patch is printed on the underside of the substrate, and eight rectangular slots are periodically arranged at intervals of 45° in the circular patch to achieve directional radiation in low frequency band and another eight rectangular slots are etched on the inner side of the circular patch in an arrangement as described above. Similarly, a ring-shaped patch truncated into eight segments is printed around the slotted circular patch, a turnstile-shaped patch is printed on the top surface of the substrate. It is worth mentioning that the turnstile-shaped patch consists of two sets of cross-shaped metal branches and eight arc-shaped branches with a radius of 24° .

The proposed pattern reconfigurable antenna is classified into four stages and analyzed by simulation using commercial electromagnetic simulation software HFSS. The dimensional parameters of the antenna are used as variables in the simulation analysis to clarify the antenna's operating mechanism. Initially, a turnstile-shaped patch antenna with a complete circular ground plane is proposed to act as an equivalent magnetic dipole with omnidirectional radiation characteristics. As described in the design guidelines in reference [19], the appropriate radius $R1$ is selected for the antenna to enable the proposed initial antenna to operate in the desired band, and the relationship between the radius $R1$ of the turnstile-shaped patch and the operating wavelength λ_h of the antenna satisfies Eq. (1). In addition, the authors have analyzed the number of antenna arms as a significant variable in the paper, and the results have shown that the number of antenna arms has a relatively weak effect on the FBR of the antenna, and the FBR value reaches its maximum at the resonance point when the number of antenna arms is four. Nevertheless, it is worth mentioning that when the number of antenna arms increases, the operating bandwidth of the antenna becomes wider and the reflection coefficient in the passband becomes better. Consequently, in order to make the antenna obtain a broad enough bandwidth to cover more 5G NR bands, the scheme of eight antenna arms is adopted in this paper. Next, according to the complementary concept, an electric dipole

Table 1. Optimized dimensions of the proposed pattern reconfigurable antenna

Parameters	R_1	L_1	W_1	R_N	R_s	R_g	W_s	L_s	a	b	d
Values	2 mm	24 mm	1.5 mm	1.3 mm	24 mm	18 mm	1.5 mm	8 mm	24°	22.5°	45°

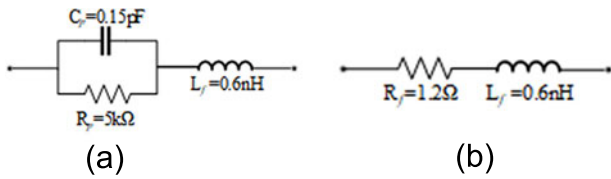


Figure 2. Equivalent circuit diagram for PIN diodes. (a) diode off-state; (b) diode on-state.

is provided to the antenna by etching radial slots on the ground plane based on the magnetic dipole that has already been introduced as shown in Fig. 3. Moreover, changing the length and width of the etched radial slot can regulate the resonant frequency of the antenna, and the specific quantitative relationship between them satisfies Eq. (2). Combining a turnstile-shaped patch that operates as an equivalent magnetic dipole and an etched radial slot ground plate that operates as an equivalent electric dipole, an antenna with a unilateral radiation pattern characteristic can be obtained.

$$2\pi L_1 = 2\lambda_g \tag{1}$$

$$2g_l + g_w \approx \frac{1}{3}\lambda_h \tag{2}$$

For the electrical reconfiguration of the antenna, a total of eight bias circuits are installed in the rectangular slots. As shown in Fig. 1(c), every bias circuit includes a 47-nH inductance for the purpose of obstructing the RF signal, a 100-pF capacitor to block DC signal and prevent the DC signal affecting the network analyzer and the antenna, a PIN diode of type Bar50-02 V from Infineon Technologies, and two metal pads for convenient connection to the DC power supply. Furthermore, the equivalent circuit diagram of the PIN diode is also given in Fig. 2, when the diode is forward biased to realize ON state with 1.5 V DC voltage, and the rectangle slot in which it is placed constitutes a closed state. On the contrary, the slot is in the open state, when the diode left unbiased. The bias circuits on the circular patch are arranged in a counterclockwise order from SW₁ to SW₈.

These eight rectangular slots are the key point to achieve the simultaneous reconfiguration of the radiation patterns in low frequency band. As shown in Table 2, when SW₁ to SW₈ are turned on one at a time in sequence, the antenna operates respectively on the state I to state VIII. Moreover, the proposed pattern reconfigurable antenna is excited by the port placed at the center of substrate, and a coaxial probe is directly connected to the turnstile-shaped patch. Then, the ring-shaped patch is coupling excited through the substrate with a thickness of 1.6 mm. The ring-shaped patch that is excited up can be regarded as a kind of NFRP unit, which is the key point to achieve the reconfiguration of radiation pattern in the high frequency band.

Design and corresponding analysis

The process of antenna structure evolution has been divided into two parts to illustrate the operating principle of the proposed antenna. The first part analyses the beneficial effects of

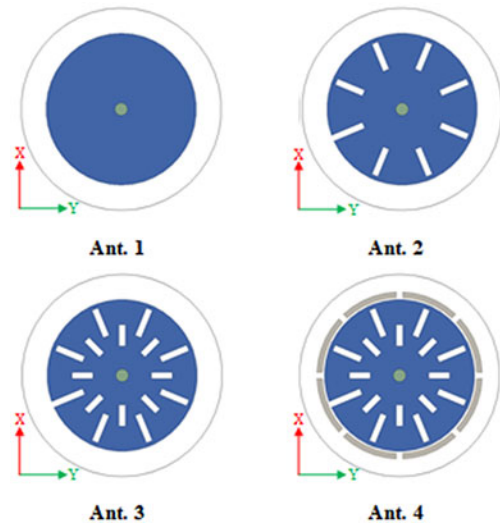


Figure 3. Evolution progress of antenna element structure.

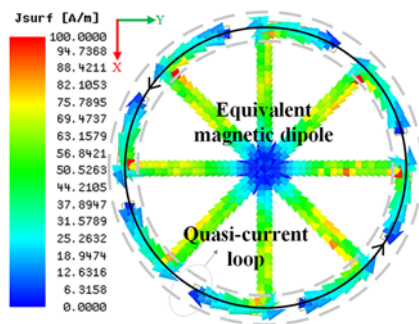
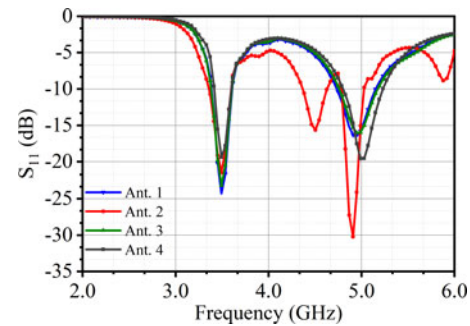
structural evolution on the reflection coefficient and impedance of the antenna, and the second part focuses on the impact of the ring-shaped patch added to the antenna on dual-band radiation patterns.

As shown in Fig. 3, in order to clearly explain the function and working principle of the rectangular slot etched on the ground plane, the evolution of the antenna ground structure is divided into four stages, and the influence curves of the four stages on the reflection coefficient and peak gain of the antenna are summarized respectively. By using this method, the effects of different slots on the ground can be distinctly distinguished. For Ant. 1, it is worth noting that the initial ground is a circular patch structure without any slots loaded. At this stage, the proposed antenna possesses a complete ground structure and the current distribution on the turnstile-shaped patch is depicted in Fig. 4. It can be clearly seen that the current is mainly concentrated on the eight arc arms of the patch, while the current intensity on the cross-lines is relatively weak. In the meantime the direction of the current is the same on all eight arc arms, and they have formed a quasi-current-loop, which is equivalent to a z-directional magnetic dipole [19]. The perimeter of the equivalent current loop, which is also the perimeter of the turnstile-shaped patch, is closely correlated to the initial operating frequency of the antenna. The principle is that as the perimeter of the turnstile-shaped patch increases, the effective current path length in the quasi-current-loop increases. As a result, the increasing effective current path causes the antenna to operate at a lower frequency. The specific quantitative relationship is given in the previously described Eq. (1).

According to the complementary theory [19], it is still required to introduce a horizontally polarized electric dipole for the proposed antenna to achieve the unilateral radiation pattern. Compared to Ant. 1, the improvement of Ant. 2 for the ground structure is only the regular rectangular slots loaded along the edge of the ground and it introduces a set of electric dipoles for

Table 2. States of the proposed antenna

States	SW ₁	SW ₂	SW ₃	SW ₄	SW ₅	SW ₆	SW ₇	SW ₈	Resonating freq. (Ghz)	Beam-direction	Gain (dBi)
I	OFF	ON	ON	ON	ON	ON	ON	ON	3.5 and 4.9	45°	4.1 and 3
II	ON	OFF	ON	ON	ON	ON	ON	ON		90°	
III	ON	ON	OFF	ON	ON	ON	ON	ON		135°	
IV	ON	ON	ON	OFF	ON	ON	ON	ON		180°	
V	ON	ON	ON	ON	OFF	ON	ON	ON		225°	
VI	ON	ON	ON	ON	ON	OFF	ON	ON		270°	
VII	ON	ON	ON	ON	ON	ON	OFF	ON		315°	
VIII	ON	ON	ON	ON	ON	ON	ON	OFF		0°	

**Figure 4.** Simulated current distribution on the turnstile-shaped patch.**Figure 5.** S_{11} of evolution progress of antenna element structure.

the antenna. The rectangular slot etched at the edge of the ground can not only introduce an electric dipole to the antenna, but also regulate the resonance point of the antenna.

Both the length and width of the rectangular slot are factors that affect the resonance point of the antenna, and they can be approximately calculated by the previously described Eq. (2) to regulate the antenna's high frequency resonance point to 4.9 GHz. It has been verified by simulation that after etching the rectangular slot, the high-frequency resonance point of the antenna is reduced from 4.95 to 4.9 GHz, while the amplitude of the reflection coefficient is reduced by 14 dB as shown in Fig. 5. On the basis of Ant. 2, Ant. 3 significantly improves the impedance matching of the antenna by loading a set of rectangular slots on the inner side of the ground with a deviation of 22.5° from the slot in Ant. 2. As shown in Fig. 6(a), the Z-parameter at the 3.5 GHz resonance point is much higher than 50 Ω, while the Z-parameter at the 4.9 GHz resonance point is lower than 50 Ω. Therefore, the process of Ant.2 to Ant.3 was produced. As known from reference [17], the impedance matching at the resonance point can be improved by the slotting method. The operation mechanism is that the surface current path on the ground is blocked by slots etched on the inner side of the ground. The comparison verification by simulation reveals that the impedance matching at the low frequency resonance point of Ant. 3 has been significantly improved shown in Fig. 6(b) and it is worth mentioning that the reflection coefficient of Ant. 3 is weakly affected by the slots shown in Fig. 5.

In Ant. 4, the innovative introduction of a discontinuous circular ring structure around the ground has been made to enhance the unidirectionality of the radiation pattern at the resonance point of the antenna and synchronize the pointing angles of the radiation pattern at the two resonance points. The discontinuous circular

ring structure is treated as a NFRP unit and utilizes a near-field parasitic coupling excitation. In other words, the main body of the antenna is fed by a coaxial cable, while the near-field resonant unit is coupled to the antenna through the FR4-epoxy substrate. The NFRP unit is printed around the antenna ground structure. In this case, the NFRP unit couples to the electric dipole introduced in Ant. 3 and absorbs a small fraction of the current. The NFRP unit part near the ground slot is more powerfully coupled and absorbs more current, and they are coupled to each other thus a more unilateral radiation pattern is produced. As shown in Fig. 7(a), before the introduction of the NFRP unit, the radiation pattern of the antenna is weakly directional and the maximum radiation directions at 3.5 GHz and 4.9 GHz are deviated by about 70°. As shown in Fig. 7(b), it can be clearly seen that after the introduction of the NFRP unit, the radiation pattern of the antenna exhibits obvious directionality and the maximum radiation directions at 3.5 GHz and 4.9 GHz are almost keep in the same direction.

In order to provide a more detailed explanation of the function of the NFRP units, a parametric analysis is conducted on the angle c between the NFRP unit and ground slot. The variation of the deflection angle c in the Ant. 4 stage with respect to the FBR at 3.5 GHz and 4.9 GHz, respectively, is shown in Fig. 8. The results show that the FBR value at 3.5 GHz reaches its peak at -8° and 13° . However the FBR value at 4.9 GHz at this point is not sharp enough to emphasize its unilateral characteristic. At the same time the deflection angle c can have a significant effect on the reflection coefficient of the antenna as shown in Fig. 10(d). Therefore, the deflection angle c is chosen as a value of 0° as an intermediate value to balance the FBR values at 3.5 GHz and 4.9 GHz. At this point the FBR for both of them takes on decent values to reflect their unilateral radiation patterns.

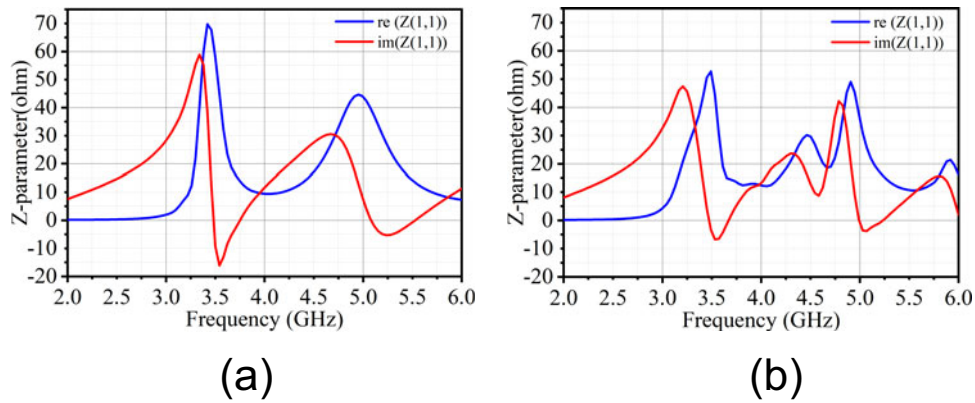


Figure 6. Simulated Z-parameter of the antenna. (a) Ant. 2; (b) Ant. 3.

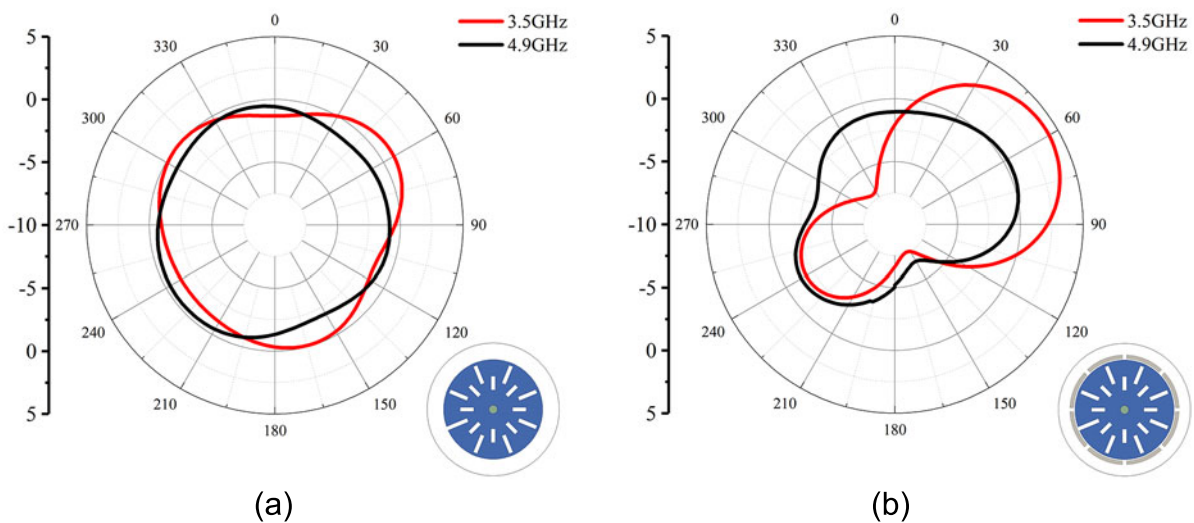


Figure 7. Comparison of radiation pattern with and without NFRP. (a) without NFRP; (b) with NFRP.

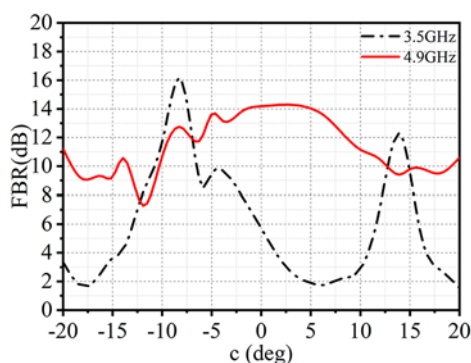


Figure 8. Effect of c on FBR.

As shown in Fig. 5, the simulated S_{11} shows that all four ground structures have two resonance points at 3.5 GHz and 4.9 GHz, which is something that we would expect. The only

difference is the amplitude of the reflection coefficient at the resonance point and the wider bandwidth of the high frequency resonance point of Ant. 4. It can be analyzed that the four evolutionary stages of the ground have a very weak effect on the reflection coefficient of the antenna. Actually the first three stages of structural evolution are designed to make the antenna radiation pattern obtain the characteristic of unilateral radiation. As to the fourth stage, which is the most important stage, the structural improvement of the antenna allows the deflection angle of maximum radiation direction at the two resonance points almost the same. Thus, the dual-band radiation patterns are synchronously adjustable.

The surface current on an antenna plays a significant role in determining its performance and characteristics. This current, which flows along the outer surface of the antenna structure, affects various aspects of the antenna's behavior. The magnitude and direction of the surface current directly influence the shape and orientation of the radiation pattern. By controlling the surface current distribution, it is possible to shape the radiation pattern to achieve desired coverage or beamforming effects.

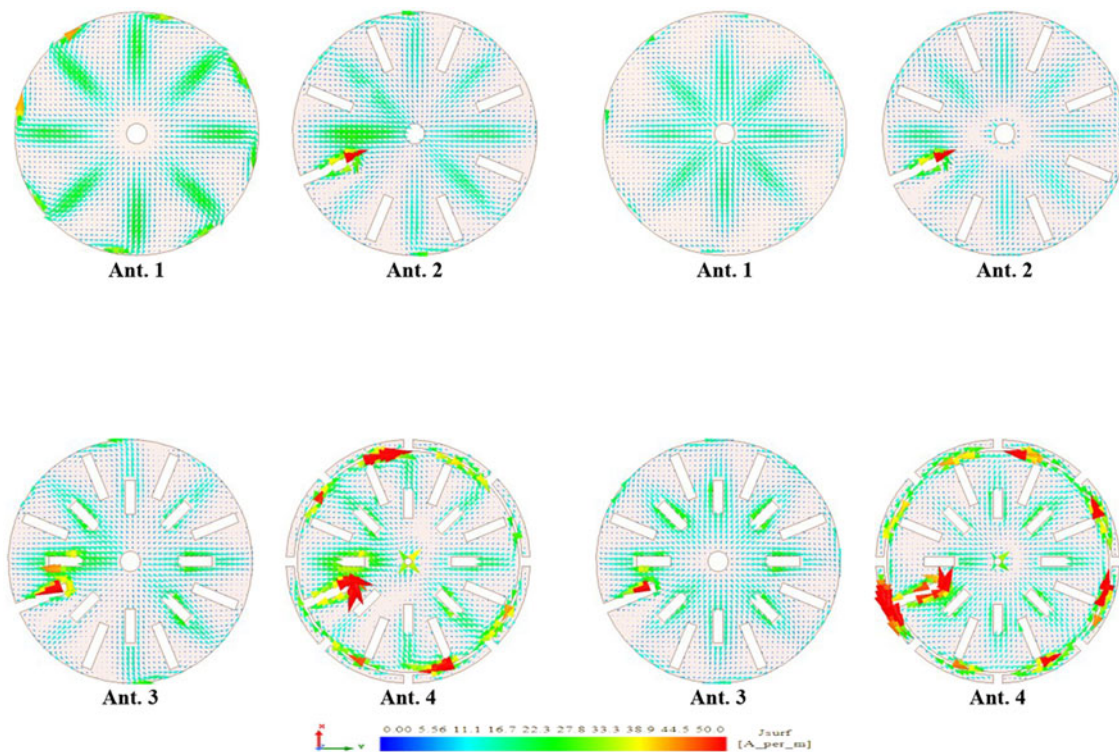


Figure 9. Simulated vector current distributions on the ground plane. (a) 3.5 GHz; (b) 4.9 GHz.

To explain the operating principle and radiation mechanism of the four antennas in a visual way, the surface current distributions of the four antennas are also given in Fig. 9. Ant. 1 in both Fig. 9(a) and Fig. 9(b) have shown that there are only regular current distributions generated by coupling with the turnstile-shaped patch on the ground plane. It can be seen from Ant. 2 in Fig. 9(a) and Fig. 9(b), after the rectangular slot is etched on the circular patch, more current is concentrated on the sides of the rectangular slot, which contrasts with the current distribution of Ant. 1. Since the radiation of current components on the two sides of the slot can cancel each other out, the slotted ground plane can be regarded as an electric dipole. In Ant. 3, slotting on the inner side of the ground plane extends the path of the concentrated current and as a result the impedance matching at the high frequency resonance point is well improved. Ant. 4 is the key to realize the reconstruction of the radiation pattern of the dual-frequency point, and the principle can be clearly observed on the current distribution graphs. In Ant. 4 of the Fig. 9(a), the 3.5 GHz current is distributed mainly on the edges of the open slot, therefore a unilateral radiation pattern is formed. The currents of different frequencies are supposed to be distributed at different locations of the antenna, however as shown in Ant. 4 of the Fig. 9(b), the 4.9 GHz current is mainly concentrated on the edges of the open slots and the NFRP units close to the slots owing to the regulation of the NFRP units. It can be observed that the 4.9 GHz current is approximately concentrated on one side of the antenna, and it is also noticeable that it is on the same side as the 3.5 GHz current. As a result, the target of simultaneous reconfigurable radiation pattern in dual-band is achieved.

Parameter analysis

The radiation pattern of the total field also depends on the relative amplitudes of the magnetic and electric dipoles. As mentioned

above, the two dipoles are entirely integrated in a single antenna in our design. Therefore, the fields radiated by them are correlated and they both depend on the dimensions of the turnstile-shaped patch and the slotted ground plane. A parameter analysis has been carried out to investigate this in detail.

Firstly, the effects of the turnstile-shaped patch are discussed. Its radius $L1$ is a key parameter to consider. Although the equation for calculating the turnstile-shaped patch radius is given in “Antenna geometry” section, the radius $L1$ calculated using the equation is just an approximate range. Therefore a parametric analysis of the radius $L1$ is conducted. It is clearly seen from Fig. 10(a) that the high-frequency resonance point decreases with increasing radius $L1$, and the effect on the low-frequency resonance point is only a weak change in the amplitude of the reflection coefficient. The antenna high frequency resonance point operates at 4.9 GHz when $L1$ is chosen to be 19.6 mm and the reflection coefficient amplitude drops to -18.3 dB.

Next, the radius Rg of the antenna ground is parameter analyzed after determining the radius $L1$ value of the turnstile-shaped patch. Changing the ground radius Rg will also only affect the high frequency resonance point of the antenna. As the radius increases, the high-frequency bandwidth in which the antenna operates becomes gradually narrower from 502 to 230 MHz and the high-frequency operating bandwidth is shifted to the left shown in Fig. 10(b). At the same time, changing the radius Rg of the ground has no effect on the bandwidth and the amplitude of the reflection coefficient at the low-frequency resonance point. Therefore the value of the radius is determined to be 18.2 mm.

Next, the effects of the NFRP unit are investigated. The NFRP unit serves as a key point for reconfigurable radiation pattern and there are a few important parameters on it. The NFRP unit radius $R2$ was parametrically analyzed and the results are plotted in Fig. 10(c). It is obvious that the radius $R2$ has a significant

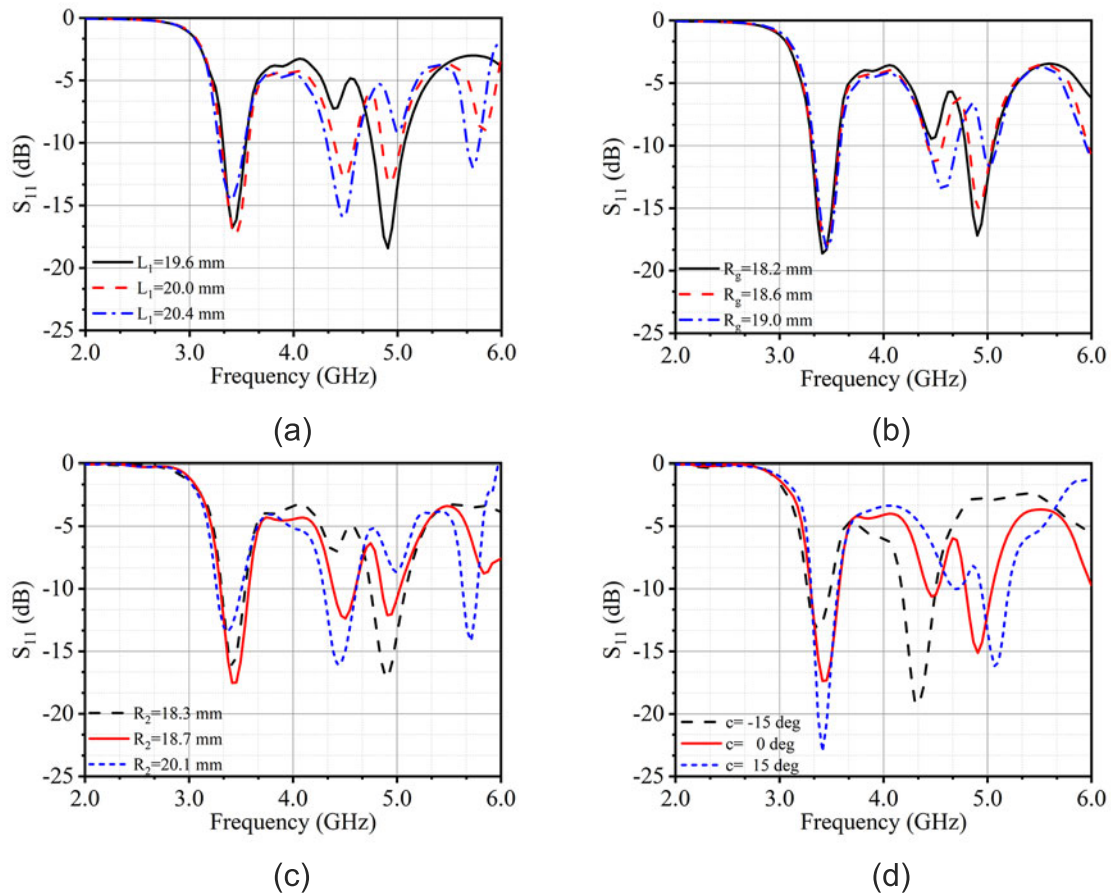


Figure 10. Effect of different parameters on simulated S_{11} of the proposed antenna. (a) L_1 ; (b) R_g ; (c) R_2 ; (d) c .

effect on the reflection coefficient of the antenna. From Fig. 1(b), it can be seen that when R_2 becomes larger, it means that the distance between the NFRP unit and the antenna ground increases. The coupling between the NFRP unit and the ground is gradually weakening, which means that the NFRP unit is losing its function. The antenna operates at the desired bandwidth when the radius R_2 is 18.3 mm. The deflection angle c has been analyzed in “Antenna geometry” section. From Fig. 10(d), it can be concluded that the high frequency resonance point of the antenna increases from 4.31 to 5.08 GHz when deflection angle c increases from -15° to 15° . Combining the considerations of Fig. 8 and Fig. 10(d), the deflection angle c is taken to be a value of 0° .

Experimental results

To validate the accuracy of the simulated results, an experimental prototype of the proposed pattern reconfigurable antenna is fabricated. An Agilent E5080A network analyzer and a Satimo Starlab near-field measurement system are used to test the performance characteristics of the proposed antenna. Figure 11(a) and Fig. 11(b) provide the photograph of the antenna prototype and measurement environment. Photographs of the front and back of the experimental prototype are shown respectively in the Fig. 11(c) and Fig. 11(d).

In this part, four of the eight states of the antenna are analyzed due to the geometric symmetry of the antenna structure. During the measurement, for the eight groups of switches described above, SW_1 is off as the first group of switches and the remaining switches are all on. Then the switch in the off state was successively changed to SW_3 , SW_5 , and SW_7 , and four sets of measurements were carried out respectively. Figure 12 illustrates the result of the comparison of measured and simulated reflection coefficient. Meanwhile, Fig. 12 also gives 3-D radiation patterns at the resonance point for each state of the antenna. As can be seen from Fig. 12, the S-parameter measurements for all four states are below -10 dB in the low band from 3.35 to 3.57 GHz, which is basically similar to the simulation results. However, the measured bandwidth of high band is from 4.83 to 5.03 GHz, which is slightly different from simulation results. The measured S-parameter curves are not stable enough in dual bands, which may be caused by the unavoidable scuff during the production and welding processes of the experimental prototype and the parasitic effect of the bias circuit. In general, the measured S-parameter results show that the proposed antenna has favorable bandwidth and can be used for 5G NR communication.

Antenna peak gain and radiation efficiency are essential parameters that determine the effectiveness of an antenna. On the one hand the peak gain refers to the maximum power radiated by an antenna in a specific direction compared to an isotropic radiator. On the other hand, the radiation efficiency represents the ability

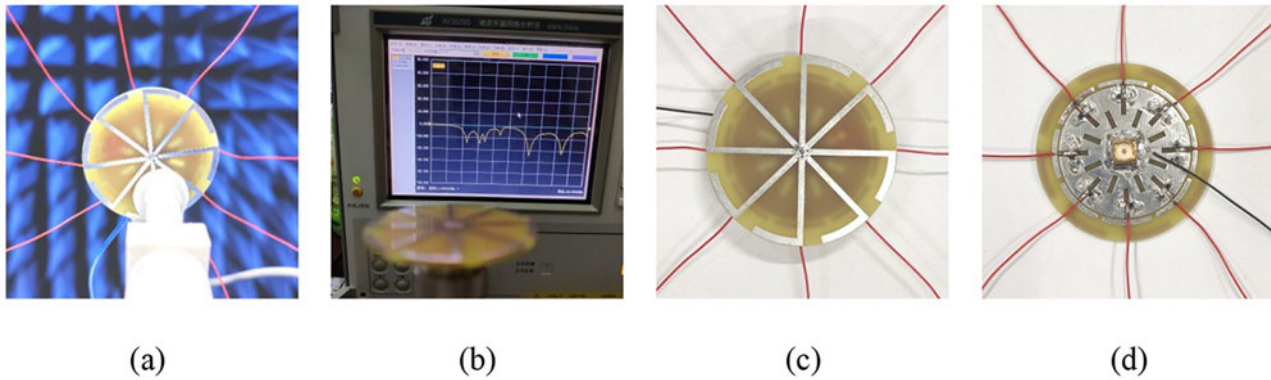


Figure 11. Prototype of the pattern reconfigurable antenna. (a) measurement environment of the prototype; (b) measurement including antenna with VNA; (c) top surface; (d) bottom surface.

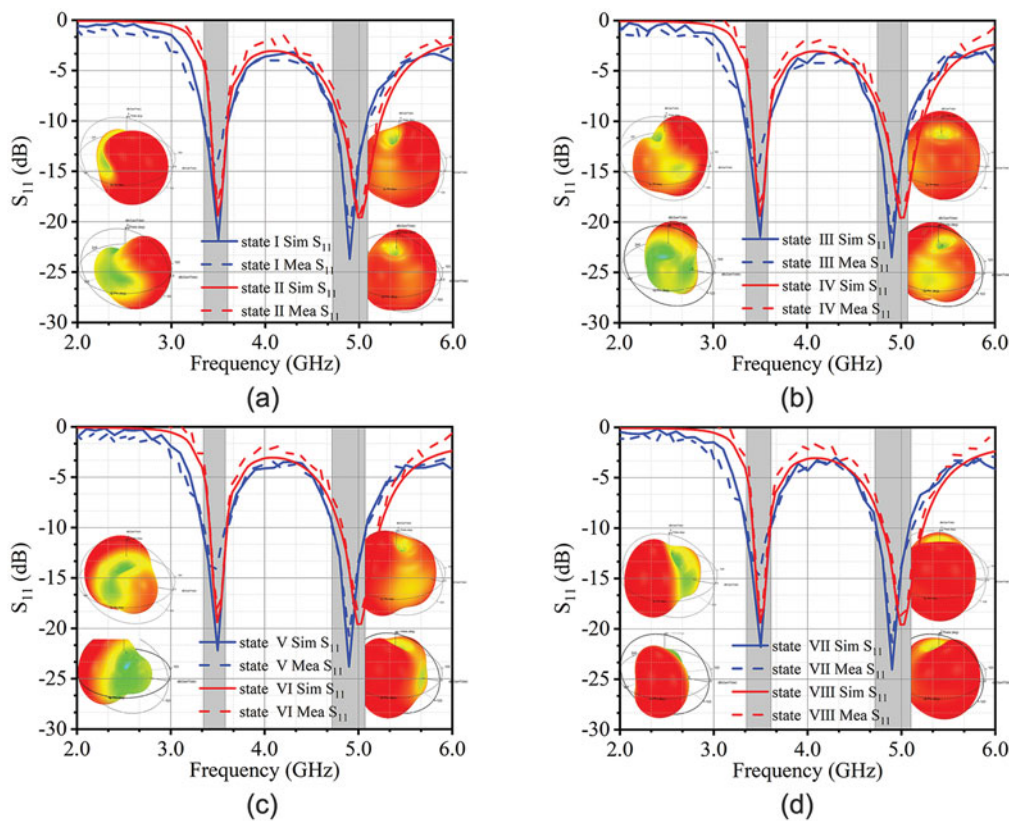


Figure 12. Comparison between simulated and measured results of S_{11} for the four of the eight states. (a) state I and state II; (b) state III and state IV; (c) state V and state VI; (d) state VII and state VIII.

of the antenna to convert input power into radiated energy effectively. Figure 13 has provided the simulation and measurement of peak gain and radiation efficiency results of the proposed pattern reconfigurable antenna. The efficiency curves in Fig. 13(a) indicate that the proposed antenna has the ability to radiate most of its energy within the operating frequency band. Simulated and measured radiation efficiency at the resonance point has reached 80%. Similarly, the simulated peak gain varies from 2.5 to 4.1 dBi over the entire operating frequency range. However, the measured peak gain deviates slightly from the simulated peak in the operating band which may be caused by errors in the placement of the

antenna during measurement. In general, the proposed antenna possesses an acceptable peak gain and radiation efficiency.

The measured results of the radiation patterns of the four states are depicted in Fig. 14 and Fig. 15. When the above four groups of switches are closed in sequence and the remaining switches are open, the measured radiation patterns on xoy-plane and yoz-plane at 3.5 GHz are shown in Fig. 14. It can be concluded from Fig. 14 that the main beam directions of the four states on the xoy-plane are separately point at 45° , 90° , 135° , 180° , 225° , 270° , 315° , and 0° , which are basically consistent with the simulated results. Moreover, the measured results also show that the

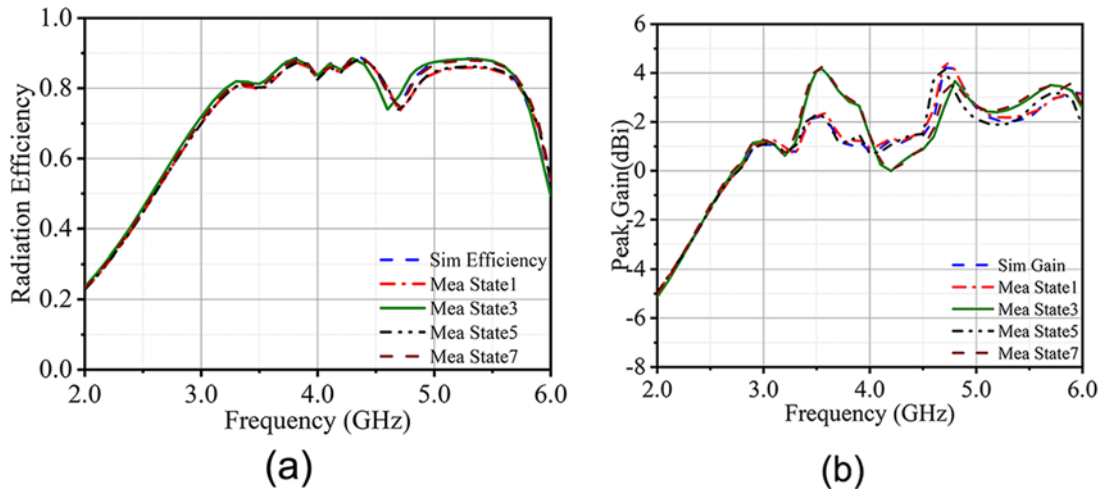


Figure 13. Simulated and measured peak gain and efficiency of the proposed antenna. (a) peak gain; (b) radiation efficiency.

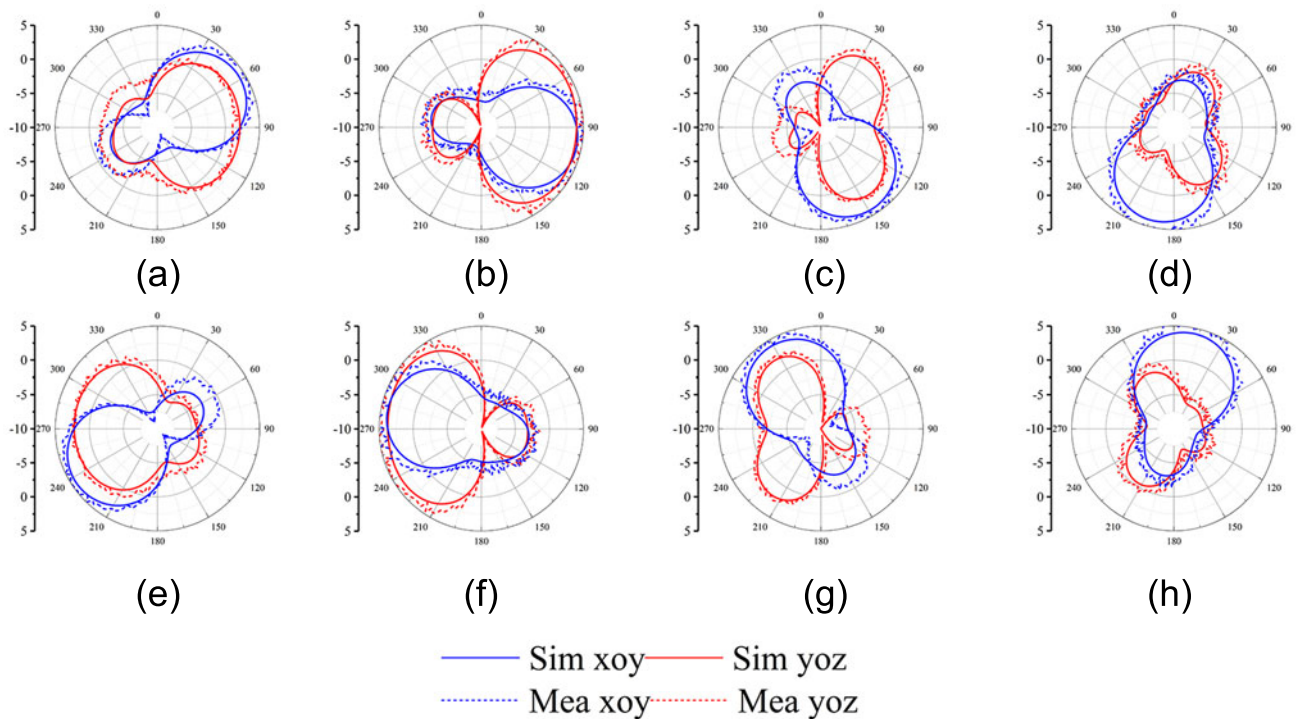


Figure 14. Simulated and measured results of radiation pattern for the pattern reconfigurable antenna in yoz-plane and xoy-plane at 3.5 GHz. (a) state I; (b) state II; (c) state III; (d) state IV; (e) state V; (f) state VI; (g) state VII; (h) state VIII.

entire azimuthal plane of the proposed antenna can be covered essentially completely by the radiation pattern in the xoy plane. Meanwhile, the measured patterns on the yoz-plane at 3.5 GHz remain directional radiation with the main beam pointing at 90° and 270°.

The measured results of the radiation pattern are also shown in Fig. 15 when the antenna operates at 4.9 GHz. Similar to the case of 3.5 GHz, with the switching of the four groups of switches, the main beam of the radiation pattern in the xoy-plane radiates successively along the directions of 45°, 90°, 135°, 180°, 225°, 270°, 315°, and 0°. At the same time, the measured radiation pattern in the yoz-plane remains the directional radiation with the main beam direction at 90° and 270°.

Comparison with other already reported pattern reconfigurable antenna

To demonstrate the superiority of the performance of the antenna proposed in this paper, a comparison with some previous antennas is summarized in Table 3. As shown in Table 3, the diverse radiation modes of the antennas presented in references [16, 19] are achieved through the integration of PIN diodes on either the radiator or the feeding network. However, these antennas are constrained by a single resonance frequency band, restricting the antenna's applicability range. Next, antennas in references [14, 15, and 20] adopt loading parasitic structure technique to extend the frequency band of the pattern reconfigurable antennas, at the

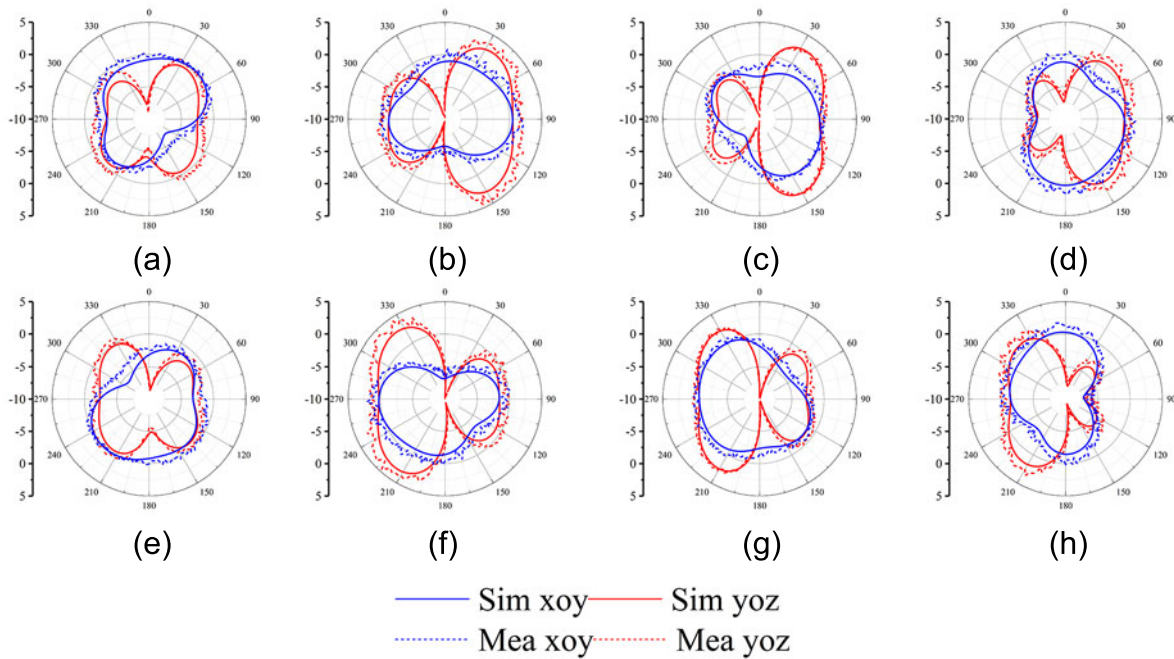


Figure 15. Simulated and measured results of radiation pattern for the pattern reconfigurable antenna in yoz-plane and xoy-plane at 4.9 GHz. (a) state I; (b) state II; (c) state III; (d) state IV; (e) state V; (f) state VI; (g) state VII; (h) state VIII.

Table 3. Comparison between reported and the proposed antenna

Ref	Impedance bandwidth(%)	Peak gain (dBi)	Efficiency (%)	Dual bands' pattern reconfigurable	Type	No. of modes	No. of diodes
14	14	4.0	>80	N	No-planar	2	0
	16	4.5					
15	0.8	1.98	>81	N	planar	3	0
	7.8	8.46					
16	5.06	5.76	>85.3	N	Planar	3	0
17	2.9	2.9	>81	N	Stacked	4	8
	2.0	4.8					
18	2.8	3.2	>74	Y	Stacked	4	8
	4.1	5.2					
19	15	3.23	>83	N	Planar	4	4
20	12.2	6	>73	N	Stacked	2	0
	9.8	7.5					
21	4.05	3.5	>44	N	No-planar	4	4
22	15	4.98	>93	N	Stacked	4	0
This work	7.5	3.6	>74	Y	Planar	8	8
	5.1	4.2					

same time these antennas are characterized by high gain and high radiation efficiency. However, these antennas are only capable of realizing pattern reconfigurable in only one band and have few reconfigurable modes. Similarly, in references [17 and 18], some antennas with dual band characteristic and dual band's pattern reconfigurable characteristic are presented, but the complexity of

the antenna structure increases. Antennas proposed in references [21 and 22] have satisfactory amount of reconfigurable patterns as well as efficiency, but none of them can realize dual-band pattern reconfigurability. In this work, the authors simplified antenna structure and combined the dual band and reconfigurable characteristics of the pattern to design an antenna with impedance

bandwidth up to 7.5% and eight radiation modes, which not only improves the spectrum utilization, but also expands the antenna's application range.

Conclusion

In this paper, a dual-band patch antenna with reconfigurable pattern characteristic is investigated. The turnstile-shaped patch is printed on the top surface of the antenna. The circular patch etched with 16 rectangular slots and the discontinuous ring patch are printed on the bottom surface of the antenna. First, the introduced rectangular slots change the current distribution on the circular patch, making the low band's radiation model of the proposed antenna equivalent to a complementary mode between a magnetic dipole and an electric dipole. As a result, the antenna obtains a unilateral radiation pattern in the low frequency band. Next, the discontinuous ring patch introduced as a NFRP unit brings high-frequency response to the antenna. Besides, the NFRP unit also enhances the FBR value of the radiation pattern in the high band. Finally, the radiation patterns in both frequency bands exhibit unilateral radiation due to the eight rectangular slots and discontinuous ring patches on the periphery of the circular patch. Each rectangular slot is equipped with a bias circuit to realize the reconstruction of the directional radiation patterns in the two frequency bands. Measurement results show that the proposed antenna has favorable dual-band characteristics. The low band is from 3.39 to 3.62 GHz with an average gain of 3.6 dBi, and the high band is from 4.77 to 5.01 GHz with an average gain of 4.2 dBi. With the switching of the state of the specific diode, the measured radiation pattern in the xoy plane indicates that the antenna has eight radiation pattern models. Also the proposed antenna has good radiation efficiency and peak gain which make it suitable for 5G NR applications.

Acknowledgements. This work was supported in part by the Natural Science Foundation of Anhui Province under Grant no.2108085MF200, in part by the Natural Science Research Project of Anhui Educational Committee under Grant no.2022AH051583.

Competing interests. The authors report no conflict of interest.

References

1. Santamaria L, Ferrero F, Staraj R and Lizzi, L (2021) Slot-based pattern reconfigurable ESPAR antenna for IoT applications. *IEEE Transactions on Antennas and Propagation* **69**(7), 3635–3644.
2. Geng J, Ziolkowski R, Wang K, Zhao X, Zhou H, Chenhu G, Liang X and Jin R (2019) Dual CP polarization diversity and space diversity antennas enabled by a compact T-shaped feed structure. *IEEE Access* **7**, 96284–96296.
3. Liu J, Li J, Xu R and Zhou SG (2019) A reconfigurable printed antenna with frequency and polarization diversity based on bow-tie dipole structure. *IEEE Transactions on Antennas and Propagation* **67**(12), 7628–7632.
4. Mabrouk B, Al-Hasan M, Nedil M, Denidni TA and Sebak AR (2020) A novel design of radiation pattern-reconfigurable antenna system for millimeter-wave 5G applications. *IEEE Transactions on Antennas and Propagation* **68**(4), 2585–2592.
5. Yang G, Li J, Wei D, Zhou SG and Xu R (2019) Pattern reconfigurable microstrip antenna with multidirectional beam for wireless communication. *IEEE Transactions on Antennas and Propagation* **67**(3), 1910–1915.
6. Ouyang W and Gong X (2019) An electronically steerable parasitic array radiator (ESPAR) using cavity-backed slot antennas. *IEEE Antennas and Wireless Propagation Letters* **18**(4) 757–761.
7. Nguyen V and Jung C (2016) Radiation-pattern reconfigurable antenna for medical implants in MedRadio band. *IEEE Antennas and Wireless Propagation Letters* **15**, 106–109.
8. Wang Z, Liu S and Dong Y (2022) Low-profile multifunctional pattern reconfigurable antenna using periodic capacitor-loaded surface for 5G and beyond. *IEEE Transactions on Antennas and Propagation* **70**(5), 3277–3286.
9. Tian H, Jiang L and Itoh T (2019) A compact single-element pattern reconfigurable antenna with wide-angle scanning tuned by a single varactor. *Progress In Electromagnetics Research C* **92**, 137–150.
10. Li K and Shi Y (2018) A pattern reconfigurable MIMO antenna design using characteristic modes. *IEEE Access* **6**, 43526–43534.
11. Jin G, Li M, Liu D and Zeng G (2018) A simple planar pattern-reconfigurable antenna based on arc dipoles. *IEEE Antennas and Wireless Propagation Letters* **17**(9) 1664–1668.
12. Sharma S, Tripathi C and Rishi R (2019) Two port integrated reconfigurable microstrip patch antenna. *Progress In Electromagnetics Research C* **89**, 39–50.
13. Santasri K, Lakhindar M and Biswajit P (2016) A pattern reconfigurable antenna for WLAN and WiMAX systems. *Progress In Electromagnetics Research Letters* **66**, 183–190.
14. Liu X, Wu Y, Zhuang Z and Wang W (2018) A dual-band patch antenna for pattern diversity application. *IEEE Access* **6**, 51986–51993.
15. Yang X, Ji Y, Ge L, Zeng X, Wu Y and Liu Y (2020) A dual-band radiation-differentiated patch antenna for future wireless scenes. *IEEE Antennas and Wireless Propagation Letters* **19**(6) 1007–1011.
16. Tang M-C, Shi T and Ziolkowski RW (2015) Flexible efficient quasi-yagi printed uniplanar antenna. *IEEE Transactions on Antennas and Propagation* **63**(12) 5343–5350.
17. Yu J, Sun Y, Fang H and Li F (2020) A novel stacked patch antenna with dual band and diverse pattern characteristics. *Microwave and Optical Technology Letters* **62**, 453–465.
18. Zhou J, Yang M and Yu J (2020) Pattern reconfigurable patch antenna with dual band characteristic for WLAN & 5G applications. *Progress In Electromagnetics Research M* **98**, 147–158.
19. Ouyang J, Pan YM and Zheng SY (2018) Center-fed unilateral and pattern reconfigurable planar antennas with slotted ground plane. *IEEE Transactions on Antennas and Propagation* **66**(10) 5139–5149.
20. Gao S, Ge L, Zhang D and Qin W (2018) Low-profile dual-band stacked microstrip monopolar patch antenna for WLAN and car-to-car communications. *IEEE Access* **6**, 69575–69581.
21. Cheng G, Tian M, Zhang L and Huang Z (2023) Design of dual-port pattern-reconfigurable MIMO antenna with four operating states using the TCM. *IEEE Antennas and Wireless Propagation Letters* **22**(1) 169–173.
22. Guo L, Fang H, Sun Y, Zhao Y, Li H and Yang W (2023) A low-profile and broadband pattern-reconfigurable dielectric resonator antenna with wide spatial coverage. *IEEE Transactions on Antennas and Propagation* **71**(10) 8296–8301.



Zhonggen Wang received the Ph.D. degree in electromagnetic field and microwave technique from the Anhui University of China (AHU), Hefei, P. R. China, in 2014. Since 2014, he has been with the School of Electrical and Information Engineering, Anhui University of Science and Technology. His research interests include computational electromagnetics, array antennas, and reflect arrays.



Jianguo Ma received the B.E degree from Anhui University of Science and Technology in 2021. He is currently pursuing the M.S degree in Anhui University of Science and Technology. His current research interest includes the theory and design of reconfigurable antenna.



Wenyan Nie is a professor at Huainan Normal University. She received the B.S. and M.S degrees from Anhui University of Science and Technology in 2007 and 2012, respectively. Her research interests include computational electromagnetic methods, antenna theory and design.



Weidong Mu received the B.E degree from Anhui University of Science and Technology in 2020. He is currently pursuing the M.S degree in Anhui University of Science and Technology. His current research interest includes the theory and design of MIMO antenna.